# A Variational Vector Finite Difference Analysis for Dielectric Waveguides

Scott S. Patrick, *Member, IEEE,* and Kevin J. Webb, *Member, IEEE*

*Abstract*—**A numerical technique based on the finite difference method is developed for the analysis of lossless dielectric waveguides. This method is a variational approach using all three components of the magnetic field vector, allowing for the enforcement of the divergence condition. The dispersion characteristics and field distributions for dielectric waveguides are accurately computed. Comparisons are made between the magnetic vectorial finite difference method and a finite element method incorporating the same functional.**

## I. Introduction

THE FINITE difference method (FDM) has long been used to analyze scalar electromagnetic problems such as waveguides [1]. More recently, however, the FDM has been used to solve dielectric waveguide problems [2], as these are vector problems and can present numerical difficulties not present in a scalar TE/TM solution. FDM solutions have been generally based upon the direct solution of the wave equation [3]–[4]. Schweig and Bridges [5] used the finite-difference method to analyze dielectric waveguides, but based their solution upon a variational approach similar to that used in the finite element method (FEM).

Initial vector variationally stable FDM and FEM waveguide analyses, including the approach developed by Schweig and Bridges, were in terms of the longitudinal electric and magnetic field components ($E_z - H_z$ FDM [6], $E_z - H_z$ FEM [7]), with the most serious drawbacks being the appearance of the so-called spurious, non-physical solutions. Konrad proposed a FEM formulation in terms of the magnetic field vector ($\boldsymbol{H}$ − FEM) [8], however spurious solutions still existed in this formulation. Rahman and Davies [9] introduced a "penalty function" for the $\boldsymbol{H}$ − FEM formulation which forces the spurious modes to be higher order solutions. Koshiba, Hayata, and Suzuki [10] have used a similar approach. The spurious solutions occurred because the basis set used was not divergenceless. The nonzero penalty term for these non-physical solutions then becomes associated with higher frequencies (eigenvalues). The result is then that the lower-order modes satisfy the zero divergence condition. The divergence condition can be used to eliminate $H_z$ from the vector magnetic field formulation, resulting in a $\boldsymbol{H}_t$ formulation which should be free from spurious solutions [11]. Alternatively, when the divergence condition is used to reduce the curl-curl operator to the Laplacian form, a two-vector magnetic field equation can be formed as two scalar equations for the hybrid problem [12], [13]. This approach has been shown to alleviate spurious solution problems when the magnetic field differential equations were solved directly, but this is not a variational formulation.

We develop a numerical technique based on the FDM in terms of all three components of the magnetic field vector ($\boldsymbol{H}$ − FDM) for the analysis of lossless dielectric waveguides. The penalty function is also incorporated into the finite-difference expressions, allowing for the suppression of spurious modes in the frequency range of interest. The dispersion characteristics and field distributions for dielectric waveguides are accurately computed. The FDM has some notable advantages compared to the FEM in the analysis of waveguides, including ease of implementation and the production of the ordinary eigenvalue problem with banded matrices. This suggests investigation of the relative merits of the $\boldsymbol{H}$ − FDM to the $\boldsymbol{H}$ − FEM.

A computer program was developed which implemented the $\boldsymbol{H}$ − FDM. To demonstrate the proper operation of the software, several cases are examined. The empty waveguide's propagation characteristics for several lower order modes are examined for different meshes. Normalized fields are also examined and compared with the exact solution. Rectangular dielectric waveguide propagation characteristics and fields are compared with several other methods, including the $\boldsymbol{H}$ − FEM based upon the same functional expression. Additionally, the troublesome spurious modes present in some FDM and FEM solutions are examined for a rectangular waveguide.

## II. Finite-Differences

### *Variational Approach*

We consider a dielectric waveguide with arbitrary cross-section in the xy-plane. For a two-dimensional source-free region with Dirichlet or Neuman boundary conditions

Manuscript received October 3, 1990; revised June 17, 1991. This work was supported in part by the Semiconductor Research Corporation under contract 90-DJ-130.

S. S. Patrick is with the Fiber & Electro Optics Research Center, Virginia Tech, Blacksburg, VA 24061. He is presently performing research at the U.S. Naval Research Laboratory, Optical Sciences Division, Code 6570, Washington, DC 20375-5000.

K. J. Webb is with the School of Electrical Engineering, Purdue University, West Lafayette, IN 47907.

IEEE Log Number 9106328.

and a dependence of $\exp j(\omega t - \beta z)$, the functional [14] is

$$F = \iint_S [(\nabla \times \boldsymbol{H})^* \cdot ([K]^{-1} \nabla \times \boldsymbol{H}) - k_0^2 \boldsymbol{H}^* \boldsymbol{H} + p(\nabla \cdot \boldsymbol{H})^* (\nabla \cdot \boldsymbol{H})]\, dS. \quad (1)$$

where $k_0^2 = \omega^2 \epsilon_0 \mu_0$, $[K]$ is the relative permittivity tensor, and $p$ is the penalty coefficient, taking on constant values greater than zero. The penalty function imposes $\nabla \cdot \boldsymbol{H} = 0$ for lower order solutions. Ideally, physical solutions are negligibly affected by variations in $p$. Generally, however, as $p$ increases, the accuracy of the solution decreases while the likelihood of the appearance of spurious solutions decreases. The functional in (1) is derived in terms of $\boldsymbol{H}$, simplifying boundary conditions for dielectric waveguides since all magnetic field components are continuous across the dielectric interfaces. By expressing (1) in terms of components, FD approximations can be applied.

To apply the FDM, we follow the approach outlined by Schweig and Bridges [5]. The dielectric guide is enclosed in a "box" with metallic wall boundary conditions (either a perfect electric conductor [pec] or a perfect magnetic conductor [pmc]). The box must be sufficiently larger than the guide in order to prevent guided mode perturbation. Appropriate boundary conditions to account for symmetry can be applied to reduce computation domain. As seen in Fig. 1, for the case of a rectangular weaveguide, a quadrant is covered by a rectangular grid with the relative permittivity $K_p$ inside each element being uniform. The nodes and elements are numbered in a fashion that minimizes the bandwidth of the matrix to be solved. The node numbering scheme used is the "natural ordering by columns" approach [15]. The width of the dielectric waveguide is $a$ and the height is $b$. The grid is constructed such that the walls of the box each divide a row or column of elements into equal halves. A graded mesh is created by changing element sizes, allowing for a better representation in certain regions.

The functional is applied over each element using FD approximations with continuity of $\boldsymbol{H}$ enforced at the nodes. Consider one such element $S_p$ with width of $h_1$ and height of $h_2$. This element's contribution to the functional can be evaluated using FD approximations [6], [16] for the terms in (1). Using $i$ and $j$ to denote the $x$, $y$, or $z$ components, we have

$$\int_{S_p} H_j^2\, dS \simeq \frac{h_1 h_2}{4} (H_{j1}^2 + H_{j2}^2 + H_{j3}^2 + H_{j4}^2). \quad (2)$$

We can approximate the term

$$\int_{S_p} \left(\frac{\partial H_j}{\partial x}\right)^2 dS = \int_0^{h_2} \int_0^{h_1} \left(\frac{\partial H_j}{\partial x}\right)^2 dx\, dy$$

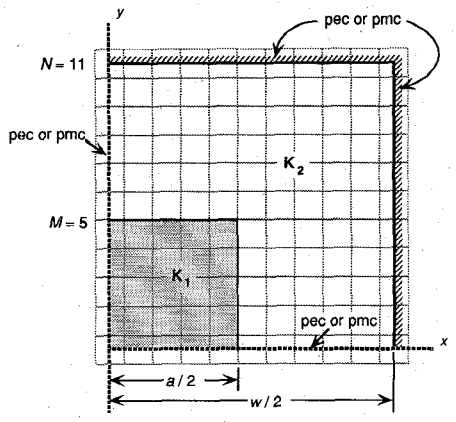


Fig. 1. The dielectric waveguide placed inside the "box" with metallic walls. The region of interest is covered by a grid of rectangular elements having uniform permittivity inside each. In this case, by exploiting symmetry, only the upper quadrant need be analyzed. For the square waveguide comparison with Goell and the $\boldsymbol{H}$ – FEM methods of solution, the outer box is made a perfect electric conductor (pec), the horizontal axis-of-symmetry is made a pec, and the vertical axis-of-symmetry is made a perfect magnetic conductor (pmc) in order to establish the dominant mode. $K_1 = 2.25$, $N = 11$, and $a = 2.0$ cm.

$$\simeq h_1 \int_0^{h_2} \left(\frac{\partial H_j}{\partial x}\right)^2 dy \simeq \frac{h_1 h_2}{2} \left[\left(\frac{H_{j4} - H_{j2}}{h_1}\right)^2 + \left(\frac{H_{j3} - H_{j1}}{h_1}\right)^2\right], \quad (3)$$

where we assume that $\partial H_j/\partial x$ has the constant value $(H_3 - H_1)/h_1$ on the segment 1–3 and the constant value $(H_4 - H_2)/h_1$ on the segment 2–4, and then use the trapezoidal rule to integrate with respect to $y$. Similarly, we can obtain

$$\int_{S_p} \left(\frac{\partial H_j}{\partial y}\right)^2 dS \simeq \frac{h_1 h_2}{2} \left[\left(\frac{H_{j2} - H_{j1}}{h_2}\right)^2 + \left(\frac{H_{j4} - H_{j3}}{h_2}\right)^2\right]. \quad (4)$$

Likewise, we approximate the term

$$\int_{S_p} H_i \frac{\partial H_j}{\partial y}\, dS \simeq \int_0^{h_1} \frac{\partial H_j}{\partial y} \int_0^{h_2} dy\, dx \simeq \frac{h_1 h_2}{4} \left[\left(\frac{\partial H_j}{\partial y} H_{i|y=h_2}\right)\Big|_{x=h_1} + \left(\frac{\partial H_j}{\partial y} H_{i|y=0}\right)\Big|_{x=h_1} + \left(\frac{\partial H_j}{\partial y} H_{i|y=h_2}\right)\Big|_{x=0} + \left(\frac{\partial H_j}{\partial y} H_{i|y=0}\right)\Big|_{x=0}\right]$$

$$\simeq \frac{h_1 h_2}{4} \left[(H_{i1} + H_{i2}) \left(\frac{H_{j2} - H_{j1}}{h_2}\right) + (H_{i2} - H_{i4}) \left(\frac{H_{j4} - H_{j3}}{h_2}\right)\right]. \quad (5)$$

Similarly,

$$\int_{S_p} H_i \frac{\partial H_j}{\partial x}\, dS \simeq \frac{h_1 h_2}{4}\left[(H_{i1} + H_{i3})\left(\frac{H_{j3} - H_{j1}}{h_1}\right) + (H_{i2} - H_{i4})\left(\frac{H_{j4} - H_{j2}}{h_1}\right)\right]$$

$$\int_{S_p} \frac{\partial H_i}{\partial x}\frac{\partial H_j}{\partial y}\, dS \simeq \frac{h_1 h_2}{4}\left[\left(\frac{H_{i4} - H_{i2}}{h_1} + \frac{H_{i3} - H_{i1}}{h_1}\right) \cdot \left(\frac{H_{j4} - H_{j3}}{h_2} + \frac{H_{j2} - H_{j1}}{h_2}\right)\right]. \quad (7)$$

Using (2)–(7), we can obtain an approximation for $F$ by summing the contributions of each element $S_p$ in the region of interest. The variational approach used is based on the Ritz procedure, with the functional being expressed as a series of functions with unknown coefficients. The expression for stationarity ($\delta F = 0$) of $F$ is found by differentiating with respect to each of the field variables, $H_{x_j}$, $H_{y_j}$, $H_{z_j}$, for every node $j$, and setting the result equal to zero. For $N^2$ elements there are $(N-1)^2$ nodes with three unknowns at each node, $H_x$, $H_y$, and $H_z$. By summing the contributions of each of the $N^2$ elements, a set of $3(N-1)^2$ linear equations is derived, which can be written as

$$\left(\frac{1}{2K_p}\boldsymbol{A} + \frac{p}{2}\boldsymbol{P}\right)\boldsymbol{X} = k_0^2\boldsymbol{B}\boldsymbol{X} \quad (8)$$

where $\boldsymbol{A}$ and $\boldsymbol{P}$ are symmetric, banded, positive-definite matrices, $\boldsymbol{B}$ is a diagonal, positive-definite matrix, and $\boldsymbol{X}$ is an ordered vector of the variables $H_{x_j}$, $H_{y_j}$, $H_{z_j}$.

Equation (8) can obviously be rewritten as

$$\boldsymbol{A}'\boldsymbol{X} = k_0^2\boldsymbol{B}\boldsymbol{X}. \quad (9)$$

By a transformation, (9) can be reduced to a simple eigenvalue problem

$$\boldsymbol{A}''\boldsymbol{X} = k_0^2\boldsymbol{X} \quad (10)$$

where

$$\boldsymbol{A}'' = \boldsymbol{B}^{-(1/2)}\boldsymbol{A}'\boldsymbol{B}^{-(1/2)}. \quad (11)$$

The matrix $\boldsymbol{A}''$ is banded and symmetric, allowing the use of a multitude of efficient algorithms to solve for the eigenvalues and eigenvectors (wavenumber and fields, respectively). The memory requirements are minimized by storing only upper banded elements of $\boldsymbol{A}''$ with a bandwidth (the number of codiagonals including the main diagonal) of $(3N + 2)$.

A program has been developed to form (10) by systematically adding the contributions of each element to form $\boldsymbol{A}$, $\boldsymbol{P}$, and $\boldsymbol{B}$. The program requires the total number of mesh elements, $N^2$; the dimensions, $h_1$, $h_2$, for each element; the relative permittivity $K_p$ at the location of the element $S_p$; the propagation constant, $\beta$; and the mode class (imposed by the type of metallic walls—pec or pmc—on each side of the "box"). The output is then the eigenvalues ($k_o$) and corresponding eigenvectors ($\boldsymbol{H}$). Details on the types of elements, local matrices, and the implementing software are in [17].

## III. Matrix Eigensystem Solution

There are many algorithms which solve the ordinary eigenvalue problem of (10). We have chosen the eigensystem routine EVESB from the well-known IMSL package. EVESB is based upon routines from the popular and accessible EISPACK eigensystem package [18]. We have used routines which were specifically designed for a banded, symmetric matrix using a solution based the rational QR method with Newton corrections [19].

It is worth noting here that the banded symmetric form of $\boldsymbol{A}''$ is one advantage of the $\boldsymbol{H}$ − FDM. Had $\boldsymbol{H}$ − FEM been used, the eigenproblem $\boldsymbol{A}\boldsymbol{X} = \lambda\boldsymbol{B}\boldsymbol{X}$ would be formed. In this case, $\boldsymbol{B}$ is a banded, rather than a diagonal matrix. Thus the ordinary eigenvalue problem cannot be formed with a banded matrix by means of a simple linear transformations. The matrix solvers of the generalized eigenvalue problem are not in as great a variety nor as accessible as those for (10).

## IV. Numerical Results and Comparisons

To verify the accuracy and versatility of the $\boldsymbol{H}$ − FDM described above, several rectangular waveguide cases are considered. More complex waveguides have been analyzed in [20].

### *Rectangular Dielectric Waveguide*

The hybrid modes of the rectangular dielectric waveguide, following the notation of [5], may be divided into four classes, depending on the symmetry of the longitudinal fields: $HE_n^{oe}$, $HE_n^{eo}$, $HE_n^{oo}$, $HE_n^{ee}$. The first superscript, $o$ or $e$, denotes the symmetry of $H_z$ with respect to the $x$-axis, the second superscript refers to the symmetry of $H_z$ with respect to the $y$-axis, and the subscript $n$ designates the order of the given mode in its class.

The square dielectric waveguide is considered. The geometry for this case along with element configuration is shown in Fig. 1. The number of elements in the width of the "metallic box," $N$, is chosen to be 11 and $M$, the number of elements in the width of the waveguide, is 5. The $\boldsymbol{H}$ − FDM is used to generate normalized $V - B$ curves, where the parameters are

$$V = k_0 a\sqrt{K_1 - K_2} \quad (12)$$

$$B = \frac{(\beta/k_0)^2 - K_2}{K_1 - K_2}, \quad (13)$$

with $K_1$ being the relative permittivity constant of the dielectric waveguide, $K_2$ the relative permittivity constant of the exterior, and $a$ the width of the waveguide. For the case at hand, $K_1 = 2.25$ and $K_2 = 1.0$. The $V - B$ curve for the dominant mode as calculated by the $\boldsymbol{H}$ − FDM is shown in Fig. 2 as the solid line. Also shown are several points taken from Goell's [21], which uses a series ex-

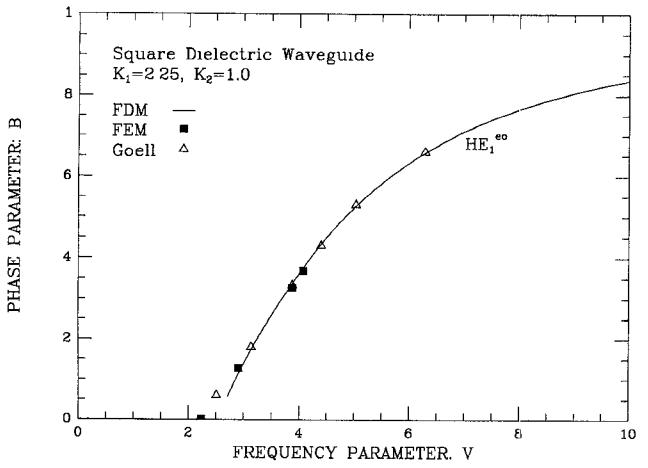


Fig. 2. The propagation characteristic for the dominant mode of the square dielectric waveguide. The solid line is the $V - B$ curve determined by the $H$ — FDM, the filled squares are values calculated by the $H$ − FEM, and the open triangles correspond to Goell's solution [21].

pansion in terms of circular harmonics. Note that the $H$ − FDM agrees very well with Goell's method. This case is also compared with a $H$ − FEM [22], [23], based on the same variational expression (1) as the $H$ − FDM. To make as valid a comparison as possible between the two methods, the sizes of the waveguide and the metallic box were the same for both the FDM and the FEM. In order to keep the order of the $A$ matrix the same, the number of elements for the FEM was 32. The penalty coefficient $p$ for both experiments was set at 1. The results for several eigenvalues are also shown in Fig. 1. Again, the results for the $H$ − FDM agree very well with those for the $H$ − FEM.

Several notable points of comparison between the $H$ − FDM and $H$ − FEM are shown in Table I. Note that the eigenvalue time of solution for the $H$ − FDM is less than the time required for the $H$ − FEM. Both the FDM and the FEM programs were run on a SUN 3/260 workstation. However, the $H$ − FDM uses an IMSL based eigensolver (EVESB), while the $H$ − FEM used in this comparison solves the eigenproblem by a subspace iteration method. Consequently, some of the computation time differences could be attributed to relative algorithm efficiency and differing mesh generation. The bandwidth is minimized for the $H$ − FDM by the global numbering scheme chosen, while some of the additional bandwidth of the $H$ − FEM can be attributed to "edge functions" which are not necessary for analysis of this particular case (edge functions are necessary for multiply-connected conducting strip problems, e.g., microstrip) and to the profile storage technique [24] used in this FEM. As mentioned, the FEM produces the generalized eigenvalue problem as opposed to the ordinary eigenvalue problem produced by the FDM, allowing for the $H$ − FDM to use a greater variety of eigensystem solvers. However, the $H$ − FEM is more flexible in the discretization of various waveguide geometries.

Consider another square dielectric waveguide is considered with $K_1$ now equal to 2.1. This time $V - B$ plots

TABLE I
COMPARISON BETWEEN $H$ − FDM AND $H$ − FEM FOR A SQUARE DIELECTRIC WAVEGUIDE $K_1 = 2.25$ AND $K_2 = 1.0$

| | $H$ − FDM | $H$ − FEM |
|---|---|---|
| Eigenequation | $AX = \lambda X$ | $AX = \lambda BX$ |
| Order of $A$ (unknowns) | 300 | 300 |
| Bandwidth of $A$ | 35 | 48 |
| Time of solution for one eigenvalue* | 33 s | 88 s |

*Includes mesh generation.

are compared with Marcatili's well-known approximation for rectangular dielectric waveguides [25]. First, we compare Marcatili's solution with the $H$ − FDM for two different sized meshes. The phase constant characteristics for the first two modes of $HE^{eo}$ class, shown in Fig. 3, are degenerate with the $HE^{oe}$ class since the waveguide is square. These correspond to the $E^x_{11}$ and $E^x_{22}$ modes in the Marcatili's notation. We see that the solution using more elements ($N = 15$), which we expect to be more accurate, has closer agreement with Marcatili's than does the $N = 11$ solution. Marcatili's closed form approximation is known to have a sharper drop-off for small $V$ than is physically correct, which is also demonstrated in Fig. 3. In general, good agreement is demonstrated. Next, the lowest eight modes for the same geometry and permittivity are considered. The $V - B$ curves for these modes are shown in Fig. 4. Correspondence between solutions is good for larger $V$, where Marcatili's approximation is considered to be more accurate.

### *Field Plots*

To compare the computed fields with other methods of solution, another square dielectric waveguide is selected, again with $K_1 = 2.1$. Here, the $H$ − FDM is compared to Schweig's $E_z - H_z$ FDM and Marcatili's solutions. Again, to make comparisons as valid as possible, $N = 15$ and $M = 8$ for both FDMs. The mode, $V$, and $B$ are shown in Table II. The dominant mode field plots for $H_z$ are shown in Figs. 5 and 6, respectively plotted as functions of $x/a$ and $y/a$. The solid lines are the fields according to Marcatili's solution and the discrete field points from both FDM's are taken from the row of nodes closest to the respective $x$- or $y$-axis. The vertical solid line represents the edge of the dielectric waveguide while the vertical dashed line shows the position of the outer metallic box. The expected sinusoidal-like behavior of the field inside the waveguide is observed, as well as the exponential decay outside the waveguide. However, both the $H$ − FDM and the $E_z - H_z$ FDM demonstrate more confined fields inside the waveguide. In Fig. 6, the $E_z - H_z$ FDM shows a drop in the field at the interface that neither the Marcatili solution nor the $H$ − FDM demonstrates. Additionally, the $E_z - H_z$ FDM shows the fields increasing slightly at the metallic box. A possible explanation for this is that Schweig and Bridges in [5] appear to have improperly emphasized the contribution of boundary elements by neglecting to eliminate the contribution of the

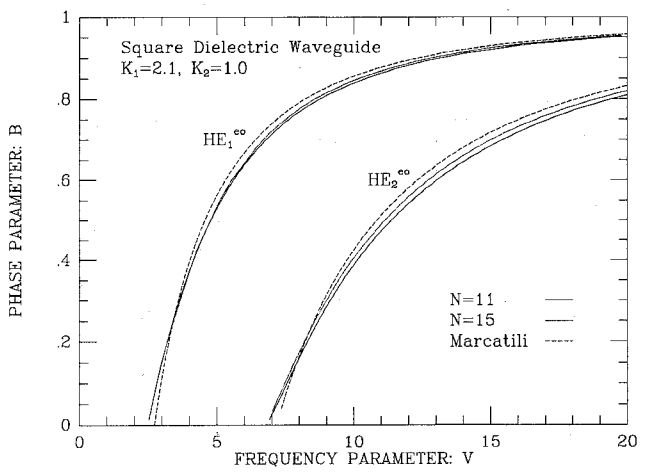


Fig. 3. $V - B$ curves for the lowest two modes of the $HE^{eo}$ class for a square dielectric waveguide with $K_1 = 2.1$. The solid line and dotted line correspond to the values calculated by the $\boldsymbol{H}$ − FDM with $N = 11$ and $N = 15$, respectively. The dashed line is Marcatili's closed-form approximation.

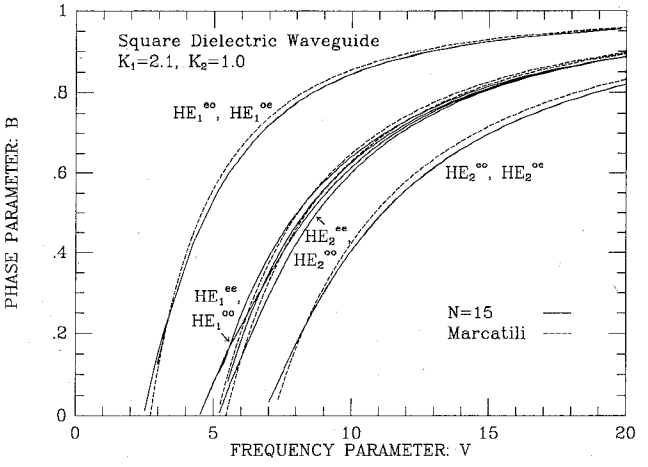


Fig. 4. Dispersion curves for the lowest eight modes of the square dielectric waveguide. The solid lines correspond to the $\boldsymbol{H}$ − FDM and the dashed lines are Marcatili's [25].

TABLE II
COMPARISON OF $\boldsymbol{H}$ − FDM, SCHWEIG'S $E_z - H_z$ FDM, AND MARCATILI'S SOLUTION FOR THE DOMINANT MODE OF A SQUARE DIELECTRIC WAVEGUIDE: $K_2 = 2.1$ AND $K_1 = 1.0$

| | Mode | $N$ | $M$ | $V$ | $B$ |
|---|---|---|---|---|---|
| $\boldsymbol{H}$ − FDM | $HE_1^{eo}$ | 15 | 8 | 5.44 | 0.59 |
| $E_z - H_z$ FDM | $HE_1^{eo}$ | 15 | 8 | 5.44 | 0.60 |
| Marcatili | $E_{11}^x$ | — | — | 5.44 | 0.58 |

functional outside the metallic boundaries. The error introduced by this is almost negligible for the eigenvalue, but in some cases produces significant error for the eigenvector at nodes near the metallic walls. Details on this are in [17].

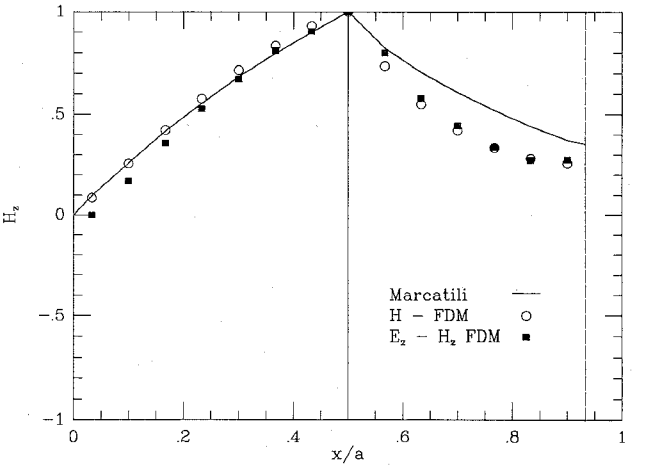


Fig. 5. Plot of the normalized longitudinal $H_z$ field as a function of $x/a$. The solid line is the field determined by Marcatili's solution, the open circles are obtained by the $\boldsymbol{H}$ − FDM and the filled squares are by Schweig's $E_z - H_z$ FDM [5]. The discrete points are taken from the row of nodes closest to the $x$-axis, where only the quartered section is considered. The vertical solid line represents the edge of the waveguide while the vertical dashed line shows the position of the outer metallic box. Parameters are shown in Table II.

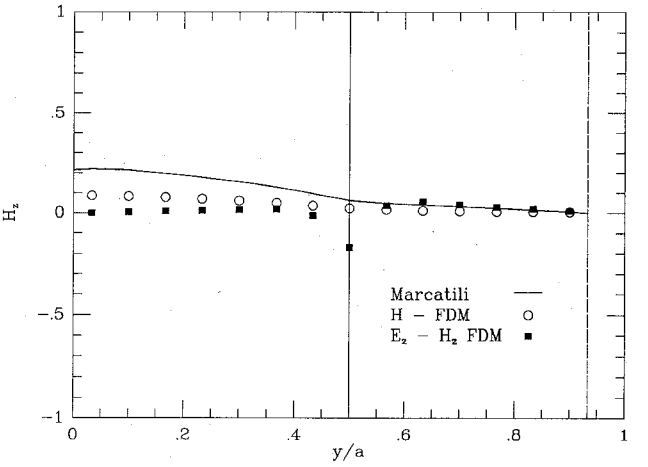


Fig. 6. Plot of the normalized longitudinal $H_z$ field as a function of $y/a$. The solid line is the field determined by Marcatili's solution, the open circles are obtained by the $\boldsymbol{H}$ − FDM and the filled squares are by Schweig's $E_z - H_z$ FDM [5]. The discrete points are taken from the row of nodes closest to the $y$-axis, where only the quartered section is considered. The vertical solid line represents the edge of the waveguide while the vertical dashed line shows the position of the outer metallic box. Parameters are shown in Table II.

### *Spurious Modes*

Spurious or non-physical modes that do not represent actual modes appear in variational-type vector methods due to the fact that the functional is a necessary, but not a sufficient condition for the true solution. By adding the penalty function, the spurious modes are moved to higher frequencies, effectively enforcing the divergence condition for the lower-order modes. It is important then to examine the effect of the penalty function on the $\boldsymbol{H}$ − FDM.

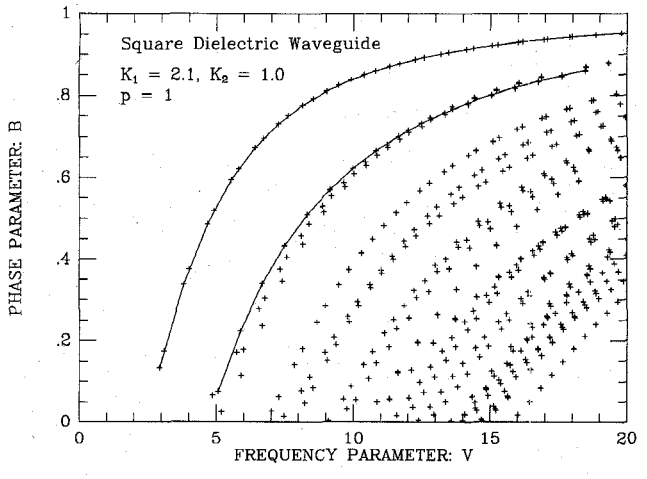


Fig. 7. Eigenvalue plot for the 40 lowest modes of the square guide ($K_1$ = 2.1) using the $H$ − FDM. No spurious solutions are present.

In using the $E_z$ − $H_z$ FDM, Schweig's variational approach contained spurious modes in the range $0.5 < B < 1.0$ [5], as did Corr's analysis [6]. When using the $H$ − FDM for the same square dielectric waveguide used by Schweig, however, no low-order spurious modes are seen for $p = 1$. Fig. 7 shows the plot of the 40 lowest modes and all correspond to physical solutions. Most cases solved by the $H$ − FEM for $p > 1$ do not produce spurious modes in the lower eigenvalue region [23], but for higher penalty numbers inaccuracies are introduced into the eigenvector. Similarly for the $H$ − FDM, no spurious modes were seen for the cases tested when $p$ was greater that 1. However, for $p < 1$, spurious modes were seen in the lower eigenvalues for both the $H$ − FEM and the $H$ − FDM. Similarly, Hayata [26] reported that for the $H$ − FEM, in general, when $p$ is large the solutions are stable but their accuracy is poorer. Likewise, for small $p$ the accuracy of the physical solutions tends to be better, but spurious solutions appear in the region of interest. The effect of the penalty number $p$ on solutions found by the $H$ − FDM appears to be similar to the effect $p$ has on its FEM counterpart.

## V. Conclusion

For the first time, a finite-difference analysis for dielectric waveguides is presented which is formulated in terms of all three components of the vector magnetic field, based upon a variational approach. The variational vectorial magnetic field formulation is convenient for inhomogeneous dielectric problems due to the ease of enforcing boundary conditions across dielectric interfaces. This finite-difference formulation produces an ordinary eigenequation having a banded, symmetric matrix for lossless dielectrics and symmetric permittivity tensors. By imposing a penalty function, therefore in essence enforcing zero-divergence for lower-order modes, spurious solutions were not a problem at lower frequencies. Compared to the finite element version of the vector magnetic field approach, the finite-difference method lends itself to a greater variety of solution algorithms, and perhaps swifter ones, due to the generation of the ordinary eigenvalue problem.

## Acknowledgment

The authors wish to acknowledge B. Slade for providing helpful comments and the comparative data from the $H$ − FEM.

## References

[1] J. H. Collins and P. Daly, "Calculations for guided electromagnetic waves using finite-difference methods," *J. Electron. Contr.*, vol. 14, pp. 361–380, 1963.

[2] S. M. Saad, "Review of numerical methods for the analysis of arbitrarily shaped microwave and optical dielectric waveguides," *IEEE Trans. Microwave Theory Tech.*, vol. MTT-33, pp. 894–899, Oct. 1985.

[3] J.-D. Decotignie, O. Parriaux, and F. Gardiol, "Birefringence properties of twin-core fibers by finite differences," *J. Opt. Commun.*, vol. 3, no. 1, pp. 8–12, Mar. 1982.

[4] C. Kim and R. Ramaswamy, "Modeling of graded-index channel waveguides using nonuniform finite difference method," *J. Lightwave Technol.*, vol. 7, pp. 1581–1589, Oct. 1989.

[5] E. Schweig and W. B. Bridges, "Computer analysis of dielectric waveguides: A finite-difference method," *IEEE Trans. Microwave Theory Tech.*, vol. MTT-32, pp. 531–541, May 1984.

[6] D. G. Corr and J. B. Davies, "Computer analysis of the fundamental and higher order modes in single coupled microstrip," *IEEE Trans. Microwave Theory Tech.*, vol. MTT-20, pp. 669–678, Oct. 1972.

[7] S. Ahmed and P. Daly, "Finite-element methods for inhomogeneous waveguides," *Proc. Inst. Elec. Eng.*, vol. 116, pp. 1661–1664, Oct. 1969.

[8] A. Konrad, "Vector variational formulation of electromagnetic fields in anisotropic media," *IEEE Trans. Microwave Theory Tech.*, vol. MTT-24, pp. 553–559, Sept. 1976.

[9] B. M. A. Rahman and J. B. Davies, "Penalty function improvement of waveguide solution by finite elements," *IEEE Trans. Microwave Theory Tech.*, vol. MTT-32, pp. 922–928, Aug. 1984.

[10] M. Koshiba, K. Hayata, and M. Suzuki, "Improved finite-element formulation in terms of the magnetic field vector for dielectric waveguides," *IEEE Trans. Microwave Theory Tech.*, vol. MTT-33, pp. 227–233, Mar. 1985.

[11] K. Hayata, M. Koshiba, M. Eguchi, and M. Suzuki, "Vectorial finite element method without any spurious solutions for dielectric waveguiding problems using transverse magnetic field component," *IEEE Trans. Microwave Theory Tech.*, vol. MTT-34, pp. 1120–1124, Mar. 1985.

[12] K. Bierwirth, N. Schulz, and F. Arndt, "Finite-difference analysis of rectangular dielectric waveguide structures," *IEEE Trans. Microwave Theory Tech.*, vol. MTT-34, pp. 1104–1114, Nov. 1986.

[13] N. Schulz, K. Bierwirth, F. Arndt, and U. Köster, "Finite-difference method without spurious solutions for the hybrid-mode analysis of diffused channel waveguide structures," *IEEE Trans. Microwave Theory Tech.*, vol. 38, pp. 722–729, June 1990.

[14] M. Koshiba, K. Hayata, and M. Suzuki, "Vectorial finite-element method without spurious solutions for dielectric waveguide problems," *Electron. Lett.*, vol. 20, pp. 409–140, May 1984.

[15] S. Selberherr, *Analysis and Simulation of Semiconductor Devices*. New York: Springer-Verlag Wien, 1984.

[16] E. Butkov, *Mathematical Physics*. Reading, MA: Addison-Wesley, 1968.

[17] S. S. Patrick, "Finite-difference analysis of dielectric waveguides: a variational approach in terms of the magnetic field vector," M.S. thesis, University of Maryland, College Park, 1990.

[18] B. S. Garbow, J. M. Boyle, J. J. Dongarra, and C. B. Moler, *Matrix Eigensystem Routines—EISPACK Guide Extension*. New York: Springer-Verlag, 1977.
[19] C. Reinsch and B. Bauer, "Rational QR transformation with Newton shift for symmetric tridiagonal matricies," *Numer. Math.*, vol. 11, pp. 264–272, 1968.
[20] S. S. Patrick and K. J. Webb, "Behavior of a magnetic-field vector-based FD analysis for optical waveguides," *IEEE Trans. Magn.*, vol. 27, July 1991.
[21] J. Goell, "A circular harmonic computer analysis of rectangular waveguides," *Bell Syst. Tech. J.*, vol. 48, pp. 2133–2160, Sept. 1969.
[22] G. W. Slade and K. J. Webb, "A vectorial finite element analysis for integrated waveguide," *IEEE Trans. Magn.*, vol. 25, pp. 3052–3054, July 1989.
[23] G. W. Slade, "Finite element analysis of integrated waveguides," M.S. thesis, University of Maryland, College Park, 1989.
[24] K.-J. Bathe and E. L. Wilson, *Numerical Methods in Finite Element Analysis*. Englewood Cliffs, NJ: Prentice-Hall, 1976.
[25] E. A. J. Marcatili, "Dielectric rectangular waveguide and directional coupler for integrated optics," *Bell Syst. Tech. J.*, vol. 48, pp. 2071–2132, Sept. 1969.
[26] K. Hayata, M. Eguchi, M. Koshiba, and M. Suzuki, "Vectorial wave analysis of side-tunnel type polarization-maintaining optical fibers by variational finite element," *J. Lightwave Technol.*, vol. LT-4, pp. 1090–1096, Aug. 1986.

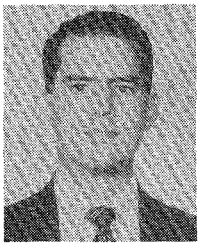

**Scott S. Patrick** (S'88–M'89) was born in Knoxville, TN in 1963. He received the B.S. degree from Tennessee Technological University, Cookeville, TN, in 1987 and the M.S. degree from the University of Maryland, College Park, in 1990, both in electrical engineering.

He joined the Fiber & Electro-Optics Research Center at Virginia Tech, Blacksburg in 1989 and is currently performing research at the Naval Research Laboratory in Washington, DC on low-frequency fiber-optic magnetic sensors. His current interests include sensor array signal processing and transducer modeling.

**Kevin J. Webb** (S'81–M'84) received the B.Eng. and M.Eng. degrees in communication and electronic engineering from the Royal Melbourne Institute of Technology, Australia, in 1978 and 1983, respectively, the M.S.E.E. degree from the University of California, Santa Barbara, in 1981, and the Ph.D. degree in electrical engineering from the University of Illinois, Urbana, in 1984.

From 1984 until 1989 he was an Assistant Professor in the Electrical Engineering Department at the University of Maryland, College Park. He is now an Associate Professor in the School of Electrical Engineering, Purdue University, West Lafayette, IN. His current research involves the study of high speed interconnects, quantum electronic devices, and diffractive gratings.